Optics Communications 478 (2021) 126393

Contents lists available at ScienceDirect

Optics Communications

journal homepage: www.elsevier.com/locate/optcom

Comparative analysis between nanorods and nanowires by using depolarized and diffuse light

Paulo Valente [a,*], Andrés Seré [a], Carlos J. Pereyra [a], Lucía Campo [a], Enzo Spera [a], Judith Castillo [b], Samuel A. Helvia [b,c], Rodrigo del Río [b,c,d,e], Daniel Ramírez [e], Gonzalo Riveros [e], Katherine Álvarez [e], Bárbara González [e], Ricardo E. Marotti [a], Enrique A. Dalchiele [a]

[a] Instituo de Física, Facultad de Ingeniería, Universidad de La República. Julio Herrera y Reissig 565, Piso 6. C.P. 11300, Montevideo, Uruguay
[b] Departamento de Química Inorgánica, CIEN UC, Pontificia Universidad Católica de Chile, Santiago, Chile
[c] Instituto de Física, Pontificia Universidad Católica de Chile, Avenida Vicuña Mackenna, 4860, Santiago, 6904411, Chile
[d] Centro de Nanotecnología y Materiales Avanzados CIEN-UC, Pontificia Universidad Católica de Chile, Chile
[e] Instituto de Química y Bioquímica, Facultad de Ciencias, Universidad de Valparaíso, Avd Gran Bretaña 1111, Playa Ancha, Valparaíso, Chile

ABSTRACT

Changes in the polarization state of light due to its interaction (reflection and transmission) with samples of CuSCN nanorod and ZnO nanowire arrays are analyzed and compared following a recently proposed technique (Valente et al., 2019). The determination of the degree of polarization and measurements of diffusive light are used to investigate the influence of the morphology of nanorods and nanowires on the optical properties. It is shown that the CuSCN nanorods are better than ZnO nanowires to preserve polarization, although the degree of polarization decreases with the lengths for both materials. It is shown that the degree of polarization correlate with the diffusive light, which allow an estimation of the large scale uniformity of the samples. However, it is also shown that the loss of polarization quality can be present even in absence of diffusion, which indicates that the interferometric effect on the nanoscale should be an important cause of the depolarizing effect.

1. Introduction

The greatest interest on the so called nanostructured materials (nanomaterials for short) relies on its interesting properties, for example the increase of area–volume relation that improves the light penetration. Another important feature concerns the shape of the nanostructures. The cylindrical shapes are referred to nanowires (NWs) and nanorods (NRs), depending on the aspect ratio defined as the relation L/D, where L and D are the nanowire length and diameter, respectively. For instance, NRs and NWs are considered those exhibiting aspect ratio values lower and greater than 5, respectively. They can be built by different electrochemical methods and of several materials, especially with semiconductors. Both features make these materials mainly suited not only for solar-cell applications, but also for other optical applications.

Among the semiconducting materials, copper (I) Thiocyanate (CuSCN) [1–3] is a pseudohalide that has been treated as a candidate for hole transporting material (HTM), because of its very small hole effective mass and normal mobility. It has a wide bandgap energy (3.6–3.9 eV) and exhibits high optical transparency in the visible wavelength region [2,4,5] together with p-type conductivity. CuSCN NR arrays offer new possibilities to fabricate nanostructured inverted solar cells, starting from the formation of nanostructured p-type electrode [6]. In fact, CuSCN NR arrays have been also employed in dye-sensitized solar cells [6] and in infrared photodetectors [7] with very good results. These facts encourage experiments to look at the polarization properties of this material.

Another useful semiconducting material is Zinc Oxide (ZnO), that is a wide bandgap semiconductor with a direct bandgap energy of about 3.37 eV and high exciton binding energy (60 meV) at room temperature [8], that can be built in a variety of nanostructures [9–11]. ZnO nanowires (ZnO-NWs) can be grown by several methods [12–16]. Among them, electrochemical deposition [17–28] offers some advantages, such as low growth temperature, simple and low cost process without the need of vacuum systems for preparing ZnO nanorods with high crystalline quality.

On the other hand, light polarization can only be analyzed by the interaction with a birefringent material medium. This class of materials (usually crystals) has two different refractive index which is defined by the arrangement of the crystalline structure, leading to different propagation velocities (and eventually directions) for the orthogonal polarization components. These crystalline materials are largely used in several applications and correspond to the fundamental optical elements used in experiments involving polarization, like those described below.

* Corresponding author.
E-mail address: pvalente@fing.edu.uy (P. Valente).

https://doi.org/10.1016/j.optcom.2020.126393
Received 14 April 2020; Received in revised form 27 July 2020; Accepted 17 August 2020
Available online 20 August 2020
0030-4018/

In this sense, nanomaterials have been proposed as "external" macroscopic birefringent materials. It was shown that arrays of very well aligned carbon nanotubes lead to important birefringence [29], as a cause of symmetry breaking. Muskens et al. [30] have shown large birefringence in GaP nanowires. Chen et al. [31] observed the same effect using slanted ZnO nanowires grown almost horizontally with respect to the substrate. The parallelism and macroscopic homogeneity of the sample are fundamental to lead to a coherent interaction of the light wavefront and the material surface. In these cited cases, the birefringence of the bulk material is very small, which indicates that the nanostructures are the responsible for the symmetry breaking in the light-material interaction. It is argued that the elongated shape of the nanowires makes the interaction with the field to be different for orthogonal polarization components, similarly to a grid of wires may act as a polarizer filter for microwaves [32–34].

In general, the changes in the polarization state of light due to transmission (or reflection) are governed in essence by the Fresnel laws, which are correctly applied for uniform surfaces [32,35]. It is well known that the roughness at micrometric scales is a natural cause of diffusive light and loss of polarization [36].

However, the behavior of light polarization after interaction with nanomaterials is an open subject, specially concerning disordered materials. It was recently shown an experiment in which the measurements of the Stokes parameters (SP) of the transmitted light was applied to a set of ZnO nanowires grown directly onto the FTO substrate [37], consisting of a disordered material. It was observed that the inhomogeneities disturb macroscopic polarization, that induces no trivial changes on the polarization state.

The aim of this work is to explore the depolarizing effect previously reported [37] in a different material (CuSCN-NR). The results are then compared to previous results on ZnO. The correlation between polarization degradation and scattered light is discussed. Furthermore, early works on these materials [28,38–40] give focus on the preparation methods and the optical properties close to the bandgap, that is close to 3 eV. Complementary, the wavelength used in the present work is at 785 nm, a region where both materials are almost transparent. Since the knowledge about polarization properties of nanomaterials is very recent, this work helps to understand the role of length, uniformity and incidence angle on optical properties.

Considering these arguments, the setup explained in the next section has been applied to 3 sets of semiconductor nanostructured samples: SS(i) A set of CuSCN nanorod arrays (CuSCN-NRs); SS(ii) a set of ZnO nanowire arrays grown onto bare SnO_2:F/glass (FTO) substrates (ZnO-NWs); and SS(iii) a set of samples of ZnO nanowire arrays grown onto four different FTO substrates with previously prepared over a ZnO seed layer (ZnO-SL). For all samples, the dependence of the light polarization and the diffuse light with the morphology of the sample is analyzed and compared. Taking in account these differences, it is expected the present results contribute to the search for polarization-sensitive materials at the nanoscale. Furthermore, as the dimensions of the nanostructures can be a smaller or similar to the light wavelength, geometrical and undulatory models are not easily applied, which reinforces the need for experiments.

2. Methods and materials

2.1. Polarization measurements

In Fig. 1 it is shown the experimental setup. It is very similar to the one presented in [37], upgraded to detect the reflected beam. A diode laser (DL), with constant power and wavelength equal to 785 nm, is used as the light source. A neutral density filter was used to adjust the light intensity incident on the sample and a polarizer (extinction ratio 1/500) defines a incident polarization state as perfect as it is possible. The sample is positioned on a goniometer, so the incident angle can be varied. For each incident angle, the detector is re-aligned

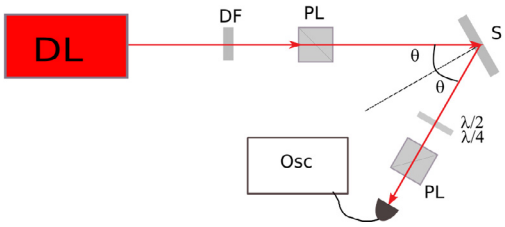

Fig. 1. Optical setup suitable for measurement of the Stokes parameters on the reflected beam. DL: Diode laser at 785 nm. DF: density filter; PL: Polarizer; S: Sample; $\lambda/2$: half-wave-plate. $\lambda/4$: quarter-wave-plate.

in order to observe only the specular reflection. The outcome light crosses a polarization analyzer (a set of wave-plate-retarder and a polarizer), which allows the measurement of the Stokes parameters $\mathbf{S} = (S_0, S_1, S_2, S_3)$, defined by

$$S_0 = I_x + I_y \tag{1}$$

$$S_1 = I_x - I_y \tag{2}$$

$$S_2 = I_{x'} - I_{y'} \tag{3}$$

$$S_3 = I_{\sigma+} - I_{\sigma-} \tag{4}$$

where each I_j represents the transmitted light intensity corresponding to a specific combination of the waveplate and polarizer. This set of measurements determines the state of polarization. Furthermore, the degree of polarization V, defined as

$$V = \frac{\sqrt{S_1^2 + S_2^2 + S_3^2}}{S_0}, \tag{5}$$

is a measurement of the polarization quality: for unpolarized light (natural light) $V = 0$ and for a perfect polarized light $V = 1$. In Ref. [37] is exposed a detailed description of the technique and its application to the samples of group (ii) mentioned above, where the transmission was measured.

2.2. Measurements of diffusive light

Total and diffuse components of the transmitted light of the samples were measured. A halogen lamp (Ocean Optics HL 2000) was used as a source of optical excitation. The excitation signal was coupled and directed to the sample by an optical fiber and a collimator (fiber core size of 1000 μm). An integrating sphere (Gigahertz-Optik UPB 150-ART) was used to obtain the optical signals. The integrated signals were coupled with another optical fiber (fiber core size of 200 μm) into a spectrometer (Ocean Optics S2000). Total and Diffuse components of the transmitted light (TT and DT respectively) were measured following standard procedures [38,41]. In these measurement, the beam transmitted by the sample is directed inside the integrating sphere and redirected into the second optical fiber after integration in the sphere. If all the ports of the integrating sphere are closed the total amount of transmitted light is measured (I_T). However, if the port in the beam direction is open with the light trap accessory then only the diffuse transmission is measured (I_D). By measuring the amount of incident light, the reference for the calculation of the transmittance is obtained (I_0). Finally, the transmittances are obtained as $TT = I_T/I_0$ and $DT = I_D/I_0$. From both signals, the fraction of diffuse to total transmitted light or Haze (HT) spectra can be calculated as HT = DT/TT. With this procedure the Haze of samples SS(ii) and SS(iii) were obtained.

Total and Diffuse reflectance (RT and RD respectively) were measured with another integrating sphere (Ocean Optics ISP-REF) which includes a tungsten lamp as optical source. In this case, the configuration of the integrating sphere allows the obtention of the total reflection or diffuse reflection signals simple by switching the light trap port of the sphere. Moreover, for the reference signal a Spectralon

Reflectance Standard (OOWS-1-SL) was used. From both total, and diffuse reflectance the reflectance Haze (HR) is calculated as HR = RD/RT. Samples of group SS(i) were studied by optical reflectance and reflectance Haze.

2.3. CuSCN nanorod arrays preparation. Set of sample SS(i)

CuSCN NR arrays have been successfully prepared via an electrochemical template-free deposition route [1,7,41–44], which has been proved to be a simple, low-temperature, and cost effective large-area deposition technique for thin films and nanostructured semiconductor materials [45,46]. Variations of the aqueous electrolyte composition and electrodeposition potentials were used to prepare CuSCN seed layers and nanorods, leading to a variety of morphological properties, always deposited onto a transparent conductive oxide (TCO). TCOs are important components for a wide range of optoelectronic technologies (photovoltaics, touch screen interfaces, etc.). Here, SnO_2:F/glass (FTO) has been employed in all samples.

Before CuSCN nanorods growth, a 120 nm CuSCN buffer layer is usually deposited on FTO substrate, both being potentiostatically electrodeposited. The presence of a buffer layer ensures a high nanorods surface density value ($\sim 10^9$ cm^{-2}). During the buffer layer deposition, a complex reduction from Cu(II) species to Cu(I) involving water, cupric ions, triethanolamine and thiocyanate ions is developed until the formation of a well covering and thin rhombohedral β-CuSCN layer.

The CuSCN nanorods morphology is strongly dependent of the thiocyanate content in the electrolyte. The diameter of these one-dimensional structures is diminished alongside the thiocyanate concentration as well as the c-axis orientation is preferred. From a chemical point of view, it is believed that competitive equilibria between thiocyanate and ethylenediaminetetraacetic acid (EDTA) plays a crucial role is stabilizing Cu(II) as electroactive species before converted into CuSCN nanorods. At high thiocyanate concentrations it is believed colloidal $Cu(SCN)_2$ is the favored species whereas at low thiocyanate concentration CuH2Y is more stable. Further, the solubility of Cu(I) under these conditions demonstrate that at low thiocyanate concentration, CuSCN is more soluble thus determining its final morphology [38,39].

2.4. ZnO nanowire arrays preparation. Set of samples SS(ii) and SS(iii)

ZnO NW arrays have been electrodeposited onto conventional transparent FTO/glass substrates. Detailed description of the sample preparation method, as well as a complete morphological, structural and optical characterization of the resulting ZnO arrays have been published elsewhere [28,47]. In brief, in these works, the effect and the importance of a previously deposited ZnO thin film seed layer onto the morphological, structural and optical properties of the resulting electrochemically grown ZnO NWs have been studied. The densely packed ZnO nanocrystals of the ZnO seed layer acts as homoepitaxial nucleation sites, favoring the growth of self-standing vertically aligned and densely ZnO nanowire arrays. In fact, the nucleation kinetics and growth of the first nuclei formed on the initial TCO substrate are critical steps that determine the physicochemical and morphological properties of the electrodeposited materials and must be understood and controlled to attain the expected properties.

Here, for the sake of comparison, ZnO NWs arrays have been electrochemically grown onto bare FTO/glass substrates (SS(ii)), and onto ZnO seed layer/FTO/glass substrates (SS(iii)). During the preparation of the samples of SS(ii), different electrochemical parameters were used leading to differences in length, diameter and density [28,37]. However, during preparation of SS(iii), most of parameters were kept constant, leading to smaller variations of the morphological parameters, especially of length.

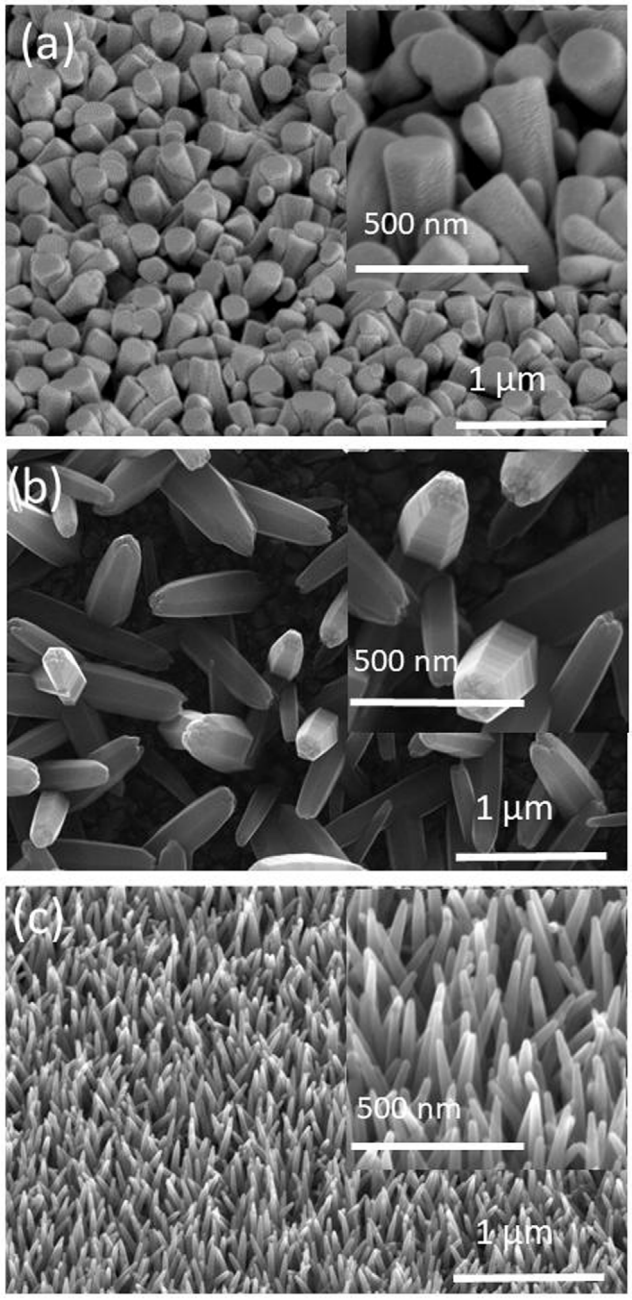

Fig. 2. Representative micrographs of each analyzed group at the same resolution scales. (a) Tilted FE-SEM micrograph view of typical CuSCN NR arrays electrochemically grown onto a CuSCN seed/FTO/glass substrate. SS(i). (b) Top view FE-SEM micrograph view of ZnO NWs electrochemically deposited onto a bare Pilkington FTO/glass substrate without ZnO seed layer. SS(ii). (c) Tilted FE-SEM micrographs of ZnO NWs electrochemically grown onto Delta commercial FTO/glass substrates with two ZnO seed layers. SS(iii). Each inset shows a high magnification view image of the corresponding sample.

3. Results

3.1. FESEM images

Fig. 2 depicts FE-SEM micrograph images of the different CuSCN and ZnO nanostructures obtained by electrodeposition. One typical image of each analyzed set was chosen to represent the morphology of the nanostructures. At the wavelength used in the experiments all the materials are transparent, so much of the differences in the optical

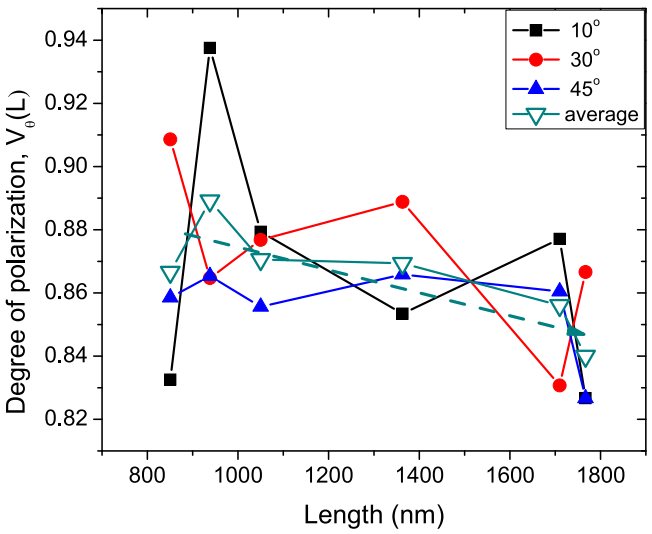

Fig. 3. Degree of polarization of the reflected beam as a function of the nanorod length for CuSCN. Different incidence angles were taken. $\theta = 10°$ (black squares), 30° (red circles) and 45° (blue up triangles). Hollow down triangles stands for the mean value between the three used angles. The dashed arrow is freehand drawing for the eyes. Only SS(i) is showed.

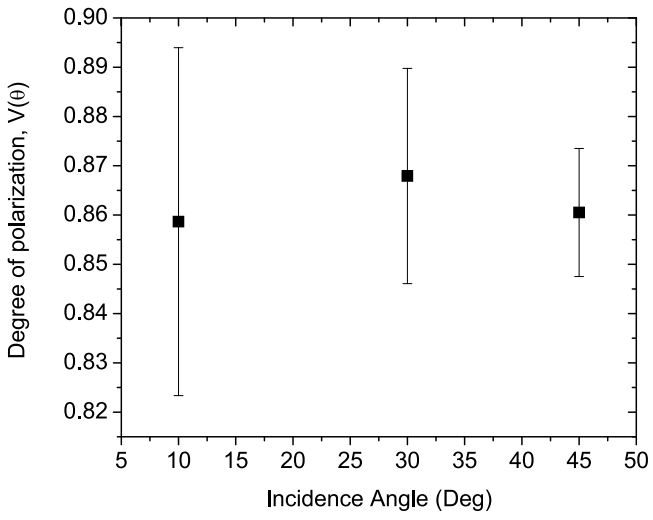

Fig. 4. Degree of polarization as a function of incidence angle for CuSCN NRs. Each point represents the average over samples of SS(i) at the same incidence angle and the error bar stands for the standard deviation of the ensemble.

properties that were observed should be caused by the differences in the sample morphology. We briefly describe some particular features of each set.

Fig. 2a shows micrographs of typical CuSCN NRs arrays electrochemically grown onto a CuSCN seed layer/FTO/glass substrate (SS(i)). Agglomerate of very dense and near orthogonal to the substrate surface CuSCN columns with marked sharp edges can be appreciated. Besides, a prismatic shape, with hexagonal face is clearly observed. These CuSCN NRs exhibited a mean diameter value of 170 nm. It is observed that the top surface of each nanorod forms a well defined plane, at the same time very few voids are left between the nanorods.

Fig. 2b and c show FE-SEM micrographs pictures of electrochemically grown ZnO NWs arrays. The micrograph presented in Fig. 2b corresponds to the ZnO NWs grown onto a bare FTO substrate (SS(ii)), whereas that depicted in Fig. 2c corresponds to ZnO NWs arrays grown onto a two ZnO seed layers (2SL)/FTO substrate (SS(iii)). ZnO NWs grown onto the bare FTO and onto (2SL)/FTO substrates exhibited a mean diameter of 160 nm and 20 nm, respectively.

In Fig. 2b it is observed the presence of poorly aligned 1D structures with large and inhomogeneous diameter distribution for the NW grown onto bare FTO substrate. Each nanowire shows a variable diameter, providing a pyramidal shape, without a defined plane in the top surface. A lot of empty space is observed between the nanowires. Fig. 2c shows well-aligned 1D ZnO nanostructures, which were obtained employing FTO substrates modified with 2SL. It forms a dense in number distribution of very thin nanowires, with very good parallelism and very small diameter, although much of empty space can also be observed.

Based on these features, it is expected that the influence of ordered and disordered arrays on the light polarization can be compared.

3.2. Polarization properties

The setup shown in Fig. 1 was used to measure the polarization properties of the reflected light of the CuSCN NRs (SS(i)). For each sample, four measurements, corresponding to Eqs. (1)–(4), were taken. For each sample, three incident angles were used $(10°, 30°, 45°)$. After that, the degree of polarization V was determined via Eq. (5) and these values were correlated to the morphological information available for the samples. It was observed that the changes in the macroscopic polarization state of the reflected light are basically random. In other words, each component of the Stokes vector suffers a small and unpredictable change, leading to an elliptical polarization for the outcome light. However, the degree of polarization may show interesting correlations to the sample morphological parameters. In Fig. 3 it is plotted the degree of polarization as a function of the CuSCN NR lengths for three incident angles. It is also plotted the average value between the three angles for each sample (only SS(i) are shown). For very small incidence angles (10° in this case) it is possible to observe large variations between the samples and it is difficult to find out a general trend. However, for larger incidence angles, the dispersion is reduced. The average values between the three used angles reveals a decrease of polarization quality when the NRs increase in length. It is also observed that the global variation between the samples is highly reduced when the incidence angle increases. The measured values of V ranged in the interval $0.83 \leq V \leq 0.94$, showing that the CuSCN NRs disturbs very little the polarization state of the incident light. In Fig. 4 it is plotted the average value of V that was taken over all the CuSCN NR samples for each one of the incident angle. It is also presented an error bar that corresponds to the standard deviation of the ensemble. No significant variation is observed as a function of the incident angle for the mean value of V. However, it is possible to observe a significant reduction of the standard deviation as the incident angle is increased, a result that will be discussed below.

For the samples of SS(ii) the dependence with the ZnO NWs length was shown in Ref. [37] for the transmitted light. Although only the normal incidence angle was analyzed, it was observed the same general behavior: a decrease in the polarization quality as the NW length is increased. The lengths of the samples of SS(iii) were not determined. For instance, all the samples were prepared using the same electrochemical recipe, differing only in the number of seed layers applied and the substrate used. Thus no significant differences in length are expected for this group [37].

For each sample in each group the diffusive part of the transmitted and reflected light were measured and the Haze values at 785 nm were determined, as explained in Section 2.2. The results are summarized in Fig. 5. The same general trend was observed for all the three groups, showing a reduction of the degree of polarization as the Haze increases, indicating that the effect of loss of polarization is very related to the diffusive part of the light that is reflected (or transmitted) by the sample. However, some differences must be observed concerning the average value of the Haze value of each group, and its correlation to the polarization quality.

4. Discussion

For applications, an important aspect to be understood concerns the level of organization of the samples. The macroscopic polarization state can be thought as an average polarization, when light is considered as a flow of photons. The reflection and transmission on a single nanowire level should depend on the incidence angle and the polarization direction, so each photon outcoming the nanowire can have its polarization slightly changed. Hence, macroscopic birefringent materials tends to be achieved by very well aligned materials. In such a case, most of incident photons interact with the same incidence angle in each nanowire. However, for disordered materials, this coherent interaction is lost, leading to a disturbed collective state of polarization. In this sense, the degree of polarization can be thought as a measurement of the width of photon distribution in a polarization space of states. The same reasoning is valid for the relation between the diffusive and specular reflection or transmission. For very well aligned arrays the large scale spatial coherence would significantly reduce the random scattered light, since incidence angle (and so the refracted and reflected directions) can be considered constant for one array. In this sense scattered light is a natural indicative of the level of order and the determination of the Haze factor represents an interesting quantitative approach. Since the measurement of the polarization is done on the transmitted (or reflected) beam and the Haze is determined by an integrating sphere, both magnitudes are complementary and can be used to estimate the homogeneity of the sample. In contrast to the FE-SEM images, where only a very small area of the sample can be pictured at a time, the optical measurements illuminate a macroscopic region of the sample, and so best to test large scale homogeneity.

The results of Fig. 3 shows that the perturbation on the polarization increase with the length of the nanorods with a slope of $\frac{\Delta V}{\Delta L}|_{\mathrm{CuSCN}NR} = -0.03\ \mu\mathrm{m}^{-1}$. It is a very small value, when compared to the one observed for ZnO NW of SS(ii): $\frac{\Delta V}{\Delta L}|_{\mathrm{ZnO}NW} = -0.08\ \mu\mathrm{m}^{-1}$ [37]. This result indicates that the morphological differences between the samples of SS(i) generate only small perturbations on the polarization state of the outcome light. Since SS(i) is composed basically by nanorods, corresponding to small aspect ratios, this result is in agreement to previous results for ZnO (SS(ii)), where it was found that a small L/D relation tends to preserve the polarization state [37].

The analysis of Fig. 4 for CuSCN NRs shows that the differences between the samples are more significant for small incident angles. It is concluded by looking at the standard deviation for each incidence angle. This result can be understood as follows. The surface inhomogeneities are an important cause of scattered light, a fact that contributes a lot to the loss of polarization. When the incidence angle is increased, a longer NR produces some shadow on his smaller neighbor. The macroscopic consequence is the reduction of the scattered light on the NR top surface, resulting in differences on the degree of polarization. In practice, the incident wavefront will see less variations on the NR length when the incident angle increases. It should be stressed that the dependence of the scattered light on the incidence angle is much more difficult to be observed using an integrating sphere.

Now we turn the attention to the comparison between the three analyzed sets. For that, we took the average value of the Degree of Polarization ($\overline{V}$) and Haze ($\overline{H}$) for each subset.

The mean values for the Haze are $\overline{H}|_{\mathrm{ZnO}_{SL}} = 5\%$, followed by $\overline{H}|_{\mathrm{CuSCN}} = 17.7\%$, and $\overline{H}|_{\mathrm{ZnO}} = 74\%$. These differences may be understood looking at Fig. 2. For the samples of SS(ii) (Fig. 2b) the low filling fraction, the absence of parallelism and the pyramidal shape, seems to contribute to provide a spatial incoherence for the incident light and so to contribute to diffuse light. In the opposed extreme, the SS(iii) (Fig. 2c) provide very small cross section for normal incidence, since the nanowire mean diameters are very small, highly parallel and normal to the surface, providing uniformity on the incidence angle. For the SS(i) samples, the high filling fraction will tend to increase the light reflected on the top surface, but the good uniformity of the surface seems to compensate these effect, resulting in moderate amount of diffuse reflection.

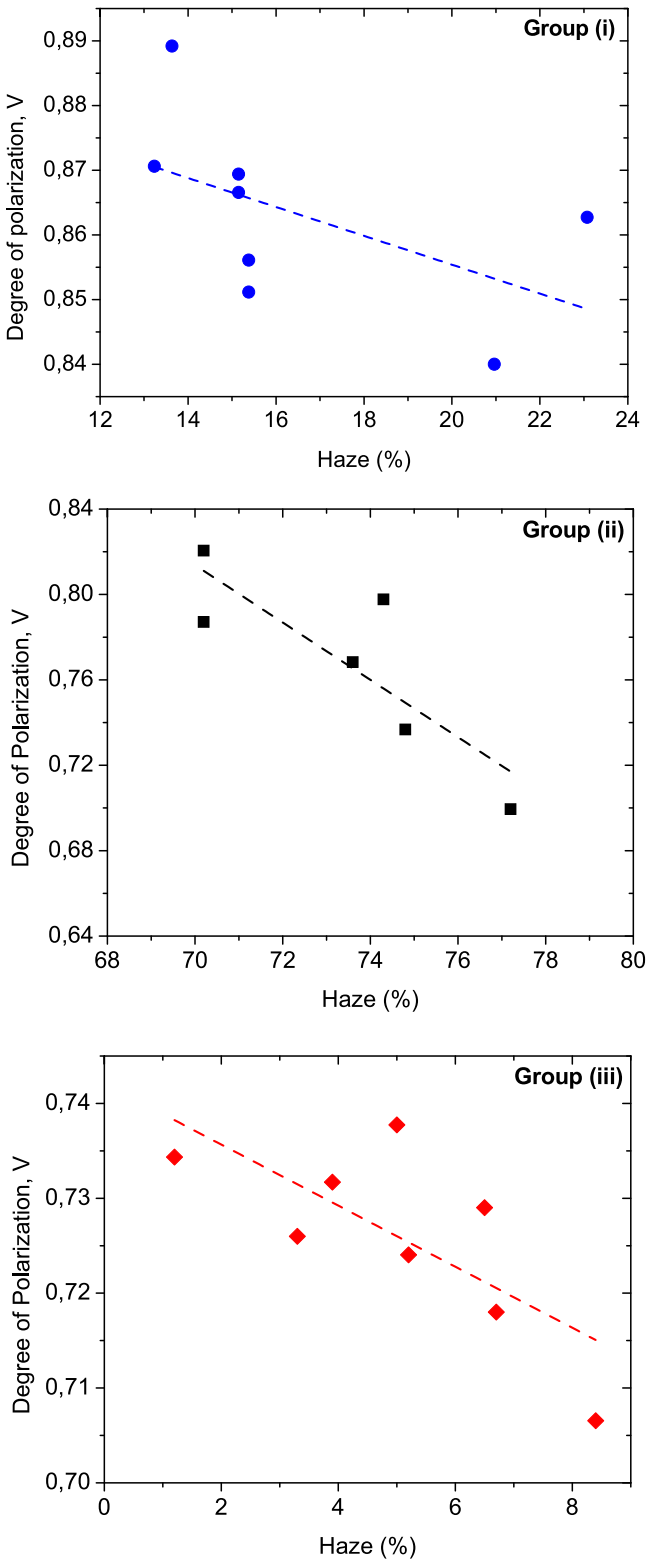

Fig. 5. Degree of polarization as a function of Haze for the three analyzed groups of samples. Blue circles for CuSCN NR (SS(i)), $R = 0.17$. Black squares for ZnO NW (SS(ii)), $R = 0.63$. Red diamonds for ZnO-SL NW (SS(iii)), $R = 0.44$. R stands for the coefficients of linear regression.

The mean values of the degree os polarization follows a different trend: For SS(i) $\overline{V}_{\mathrm{CuSCN}} = 0.86$, which is higher than that encountered

for the SS(ii) ($\overline{V}_{\mathrm{ZnO}} = 0.75$), which is similar to that encountered for SS(iii) ($\overline{V}_{\mathrm{ZnO}_{SL}} = 0.73$). These differences indicate that the loss of polarization quality is not just a collateral effect of random scattering at the surface. These results corroborate the argument presented in reference [37], in which an interference mechanism between the field that passes through the nanostructure and the neighbor field should have influence on the depolarization. In fact, it depends on the shape and dimensions of nanostructure and the material involved.

It is also noted that both groups (i) and (iii) were prepared by the application of seed layers previously to the growing process, while SS(ii) was not (see Sections 2.3 and 2.4). It clearly indicates that seed layer deposition strongly helps to introduce large scale order and this high ordering level seems to prevent light scattering. Instead, the results of the degree of polarization show that both groups of ZnO have the same average value for the degradation, which indicates that the refractive index of the material, as well as its morphology are of fundamental influence, specially the NW lengths.

However, the results of Fig. 5 show that for each analyzed group, the degree of polarization tends to decrease with the Haze value, what shows that diffusive light and the loss of polarization have a common origin, associated to the inhomogeneities of the surface. It can be concluded that once the material and the morphology is fixed, the depolarization will be accompanied by diffusion.

Finally, a comment on the case of SS(iii), where the different substrates were prepared with seed layer deposition. It was observed a small range of variations for V and also for the Haze fraction. It should be noted that the mean Haze (at 785 nm) was about 5% for this group, although the mean value for the polarization quality is very close to the observed for the SS(ii). It reinforces the idea that the loss of polarization is basically governed by the nanowire lengths.

5. Conclusions

An experiment that reveals some optical polarization properties of nanostructured materials was presented. The method was applied to a group of CuSCN nanorods and two groups of ZnO nanowires, differing between them by previous application of seed layers onto the substrate. It was found that increasing the length of the CuSCN nanorods contribute to the polarization degradation, in agreement to previous results for ZnO nanowires.

It was observed a correlation between the polarization degradation and the amount of diffuse light reflected (or transmitted) by the sample array, which enables an estimation of its macroscopic level of order.

Finally, CuSCN NRs are found to be better to preserve light polarization and the application of two seed layers on the substrate can greatly reduce the diffusive reflection (and transmission) of ZnO NW, although it does not prevent polarization degradation.

CRediT authorship contribution statement

Paulo Valente: Designed the polarization experiment, Performed the correlations, Interpret the results and write the manuscript. **Andrés Seré:** Performed the measurements of the Stokes parameters. **Carlos J. Pereyra:** Performed optical characterizations using the integrating sphere. **Lucía Campo:** Prepared the ZnO nanowires (samples Group (i)). **Enzo Spera:** Performed optical characterizations using the integrating sphere. **Judith Castillo:** Prepared the ZnO nanowires grown on seed layer (samples of Group (ii)). **Samuel A. Helvia:** Designed and supervised the preparation of samples of Group (ii). **Rodrigo del Río:** Designed and supervised the preparation of samples of Group (ii). **Daniel Ramírez:** Designed, prepared and characterized the CuSCN nanorods (samples of Group (iii)). **Gonzalo Riveros:** Designed, prepared and characterized the CuSCN nanorods (samples of Group (iii)). **Katherine Álvarez:** Designed, prepared and characterized the CuSCN nanorods (samples of Group (iii)). **Bárbara González:** Designed, prepared and characterized the CuSCN nanorods (samples of Group (iii)). **Ricardo E. Marotti:** Designed and supervised the optical characterizations. **Enrique A. Dalchiele:** Designed and supervised sample preparations.

Declaration of competing interest

The authors declare that they have no known competing financial interests or personal relationships that could have appeared to influence the work reported in this paper.

Acknowledgments

PEDECIBA – Física, CSIC, ANII (Project number: FCE-1-2014-1-104739), uruguayan agencies. Project FONDECYT 1161614, FONDEQUIP EQM 150101, CONICYT National PhD Scholarship No 21160394, Chile. D. Ramírez acknowledges to FONDECYT project grant n^o: 1141257, Chile. Antonio Saez and Joaquin Fernandez for technical support (Uruguay).

All authors contributed for writing the manuscript and approved the final submitted version.

References

[1] D. Aldakov, C. Chappaz-Gillot, R. Salazar, V. Delaye, K.A. Welsby, V. Ivanova, P.R. Dunstan, J. Phys. Chem. C 118 (2014) 16095–16103.
[2] P. Pattanasattayavong, N. Yaacobi-Gross, K. Zhao, G.O.N. Ndjawa, J. Li, F. Yan, B.C. O'Regan, A. Amassian, T.D. Anthopoulos, Adv. Mater. 25 (2012) 1504–1509.
[3] Y. Son, N.R. de Tacconi, K. Rajeshwar, J. Electroanal. Soc. 345 (1993) 135–146.
[4] M.H. Li, P.S. Shen, K.C. Wang, T.F. Guo, P. Chen, J. Mater. Chem. A 3 (2015) 9011–9019.
[5] J. Garnier, R. Parize, E. Appert, O. Chaix-Pluchery, A. Kaminski-Cachopo, V. Consonni, ACS Appl. Mater. Interfaces 7 (2015) 5820–5829.
[6] L. Sun, K. Ichinose, T. Sekiya, T. Sugiura, T. Yoshida, Physics Procedia 14 (2011) 12–24.
[7] R. Gertman, A. Harush, I. Visoly-Fisher, J. Phys. Chem. C 119 (2015) 1683–1689.
[8] U. Ozgur, Y.I. Alivov, C. Liu, A. Teke, M.A. Reshchikov, S. Doğan, V. Avrutin, S.J. Cho, H. Morkoç, J. Appl. Phys. 98 (2005) 041301.
[9] Y. Heo, D. Norton, L. Tien, Y. Kwon, B. Kang, F. Ren, S. Pearton, J. LaRoche, Mater. Sci. Eng. R 47 (2004) 1–47.
[10] M. Skompska, K. Zarębska, Electrochim. Acta 127 (2014) 467–488.
[11] B. Kumar, S.W. Kim, Nano Energy 1 (2012) 342–355.
[12] M.H. Huang, Science 292 (2001) 1897–1899.
[13] W. Lee, M.C. Jeong, J.M. Myoung, Acta Mater. 52 (2004) 3949–3957.
[14] D. Qiu, P. Yu, H. Wu, Solid State Commun. 134 (2005) 735–739.
[15] M. Susner, S. Carnevale, T. Kent, L. Gerber, P. Phillips, M. Sumption, R. Myers, Phys. E 62 (2014) 95–103.
[16] S.T. Rajan, B. Subramanian, A.N. Kumar, M. Jayachandran, M.R. Rao, J. Alloys Compd. 584 (2014) 611–616.
[17] M. Guo, C. Yang, M. Zhang, Y. Zhang, T. Ma, X. Wang, X. Wang, Electrochim. Acta 53 (2008) 4633–4641.
[18] T. Pauporté, G. Bataille, L. Joulaud, F.J. Vermersch, J. Phys. Chem. C 114 (2009) 194–202.
[19] T. Pauporté, Design of solution-grown zno nanostructures, in: Toward Functional Nanomaterials, Springer US, 2009, pp. 77–125.
[20] D. Lincot, MRS Bull. 35 (2010) 778–789.
[21] C.D. Bojorge, V.R. Kent, E. Teliz, H.R. Cánepa, R. Henríquez, H. Gómez, R.E. Marotti, E.A. Dalchiele, Phys. Status Solidi (a) 208 (2011) 1662–1669.
[22] G. Guerguerian, F. Elhordoy, C.J. Pereyra, R.E. Marotti, F. Martín, D. Leinen, J.R. Ramos-Barrado, E.A. Dalchiele, Nanotechnology 22 (2011) 505401.
[23] H. Gomez, G. Riveros, D. Ramirez, R. Henriquez, R. Schrebler, R. Marotti, E. Dalchiele, J. Solid State Electrochem. 16 (2011) 197–204.
[24] A. Tello, H. Gómez, E. Muñoz, G. Riveros, C.J. Pereyra, E.A. Dalchiele, R.E. Marotti, J. Electrochem. Soc. 159 (2012) D750–D755.
[25] H. Gómez, S. Cantillana, G. Riveros, S. Favre, C.J. Pereyra, D. Ariosa, R.E. Marotti, E.A. Dalchiele, Int. J. Electrochem. Sci. 8 (2013) 10149–10162.
[26] F.A. Catao, H. Gomez, E.A. Dalchiele, R.E. Marotti, Int. J. Electrochem. Sci. 9 (2014) 534–548.
[27] M. Berruet, D.L. Gau, E.A. Dalchiele, M. Vázquez, R.E. Marotti, J. Phys. D: Appl. Phys. 49 (2016) 215103.
[28] L. Campo, E. Navarrete-Astorga, C.J. Pereyra, A. Cuevas, R. Romero, D. Ariosa, R. Henríquez, E. Muñoz, R.E. Marotti, F. Martín, J.R. Ramos-Barrado, E.A. Dalchiele, J. Electrochem. Soc. 163 (2016) D392–D400.
[29] W.A. de Heer, W.S. Bacsa, A. Chatelain, T. Gerfin, R. Humphrey-Baker, L. Forro, D. Ugarte, Science 268 (1995) 845–847.
[30] O.L. Muskens, M.T. Borgström, E.P.A.M. Bakkers, J.G. Rivas, Appl. Phys. Lett. 89 (2006) 233117.
[31] C.Y. Chen, J.H. Huang, K.Y. Lai, Y.J. Jen, C.P. Liu, J.H. He, Opt. Express 20 (2012) 2015.
[32] E. Hecht, Optics, fourth ed., Addison'Wesley, 2002.
[33] H.E. Ruda, A. Shik, Phys. Rev. B 72 (2005).
[34] H.E. Ruda, A. Shik, J. Appl. Phys. 100 (2006) 024314.

[35] M. Born, E. Wolf, Principles of Optics, sixth ed., Cambridge University Press, 1980.
[36] V. Celli, A. Marvin, F. Toigo, Phys. Rev. B 11 (1975) 1779–1786.
[37] P. Valente, A. Seré, C. Pereyra, L. Campo, R. Marotti, E. Dalchiele, Phys. E 114 (2019) 113600.
[38] D. Ramírez, G. Riveros, K. Álvarez, B. González, C.J. Pereyra, E.A. Dalchiele, R.E. Marotti, D. Ariosa, F. Martín, J.R. Ramos-Barrado, Mater. Sci. Semicond. Process. 68 (2017) 226–237.
[39] D. Ramírez, K. Álvarez, G. Riveros, B. González, E.A. Dalchiele, Electrochim. Acta 228 (2017) 308–318.
[40] C.J. Pereyra, Caracterización de Materiales Nanoestructurados Para Celdas Fotovoltaivcas: Dispersión de la Luz y Transporte de Portadores de Carga (Ph.D. thesis), UDELAR, 2018.
[41] C. Chappaz-Gillot, R. Salazar, S. Berson, V. Ivanova, Electrochim. Acta 110 (2013) 375–381.
[42] J.H. Rhee, C.C. Chung, E.W.G. Diau, NPG Asia Mater. 5 (2013) e68.
[43] S. Sanchez, C. Chappaz-Gillot, R. Salazar, H. Muguerra, E. Arbaoui, S. Berson, C. Lévy-Clément, V. Ivanova, J. Solid State Electrochem. 17 (2012) 391–398.
[44] S. Ghosh, S.K. Sarkar, Energy Procedia 54 (2014) 777–781.
[45] S. Peulon, D. Lincot, Adv. Mater. 8 (1996) 166–170.
[46] G. Guerguerian, F. Elhordoy, C.J. Pereyra, R.E. Marotti, F. Martín, D. Leinen, J.R. Ramos-Barrado, E.A. Dalchiele, J. Phys. D: Appl. Phys. 45 (2012) 245301.
[47] J. Castillo-Rodriguez, C.J. Pereyra, P. Valente, A. Seré, R.E. Marotti, S.A. Hevia, E.A. Dalchiele, R. del Rio Quero, J. Solid State Electrochem. (2020).